INTERNAL DYNAMICS AND EMITTANCE GROWTH IN NON-UNIFORM BEAMS

O. A. Anderson
Lawrence Berkeley Laboratory
University of California, Berkeley, CA 94720

Previous analytical studies related transverse rms emittance growth in non-uniform beams to changes in the beam density profile but did not analyze the time evolution of the process.

Our new approach analyzes the internal motion of the beam and then obtains the rms emittance explicitly as a function of time. It is shown to reach its peak value explosively in about one quarter of a plasma period.

We give a uniformity criterion that determines whether or not the emittance oscillates periodically. We exhibit continuous initial density profiles that lead to discontinuous shock-like behavior and segmented (beam-merging) profiles for which the rms emittance jumps to its maximum value in one-fourth of a plasma period and remains there with essentially no further change.

Asymptotic behavior is briefly discussed.

Introduction

In 1971 Lapostolle [1] and Sacherer [2] derived rms envelope equations which were used by Lapostolle and independently by Lee [3] and Wangler [4] to obtain a differential relationship between changes in emittance and changes in self-field energy. Wangler et al. presented numerical simulations showing emittance growth in one quarter of a plasma period. However, this surprisingly rapid growth was unexplained by the analysis, which did not treat time dependence.

In the present paper, we first solve for the beam internal motion as a function of time and then calculate the moments. The rms emittance is shown to reach its peak value in about one quarter of a plasma period, in agreement with the simulations of Wangler et al.

We separate the mean-square emittance into a thermal part and a fluid-flow part. For a strongly space-charge dominated warm beam the fluid motion during the initial emittance growth is the same as for the corresponding cold beam, except for a slight change in timing.

Thus we do almost all of the analysis on cold beams, gaining mathematical simplicity. After calculating the explicit time dependence of the cold-beam emittance, we show how to incorporate the thermal part. We also discuss asymptotic thermalization of the emittance.

To simplify the formulas we will take the model (easily generalized [5]) of non-relativistic, singly charged particles propagating in vacuum. The beam energy is assumed much larger than the space-charge potential, allowing the usual approximations, that the beam particles all have the same longitudinal velocity v, and that the transverse velocities are much smaller than v.

We will treat both round beams and sheet beams. Round beams are by definition azimuthally symmetric, and sheet beams are by assumption symmetric in the direction of transverse motion, x. This symmetry means that only the upper half ($x \geq 0$) of a sheet beam needs to be considered; all x-integrals will start from zero.

We begin with the simpler case of sheet beams.

I. SHEET BEAMS

Space Charge Field

If the beam density is n(x,z), the number of particles per square cm within half-width x is

$$N_x(x,z) = \int_0^x n(x_1,z)\, dx_1. \qquad (1)$$

Poisson's equation (for singly charged ions) gives $\partial N_x/\partial x = (4\pi e)^{-1} (\partial/\partial x) E_s(x,z)$ where E_s is the x-component of the space charge field, and where the term $\partial E_{sz}/\partial z$ has been dropped. This is justified if the beam is reasonably thin; i.e., if $(kh)^2 \ll 1$ where k is the channel focusing wave number and h is the beam half-width. Integrating,

$$E_s = 4\pi e N_x. \qquad (2)$$

Particle Motion

As stated in the introduction, we will begin by analyzing cold beams; thermal motion will be included later. We consider individual particles in a uniform channel with linear external focusing:

$$x'' = -k^2 x + P N_x(x,z)/N \qquad (3)$$

where $x'' = d^2x/dz^2$, N is the half-beam line density (per cm^2), and

$$P = 4\pi N e^2/mv^2 \qquad (4)$$

is the normalized line perveance, representing total space charge.

For a cold beam the particle motion is initially laminar. We will show in the next section that it remains laminar for at least the distance $\lambda/4$, where $\lambda = 2\pi/k$.

Thus we begin with the ansatz of laminar motion over a range $0 \leq z \leq z_c$ where the critical distance $z_c > \lambda/4$ is to be calculated later. Since no trajectories cross, N_x is preserved for each particle at its position x(z).

If we write ξ for the initial position of the particle that is currently at x(z), then $N_x(x,z) = N_x(\xi,0)$ for all x in the laminar range of z, so that the space-charge term in Eq. (3) is constant. Using the abbreviation $N_x(\xi,0) = N_x(\xi)$, we define the equilibrium position

$$x_e(\xi) = (P/k^2)\, N_x(\xi)/N \qquad (5)$$

and get the linear equation

$$x'' + k^2 (x - x_e(\xi)) = 0. \qquad (6)$$

For the initial condition $x'(\xi) = 0$, the solution is

$$x(\xi,z) = x_e(\xi) + (\xi - x_e(\xi)) \cos kz. \qquad (7)$$

Crossing of Trajectories

Laminar motion ceases if two beam elements with initial separation $d\xi$ are later separated by $dx = 0$; i.e., it ceases at the distance z_c where the derivative $dx(\xi,z_c)/d\xi$ vanishes. From Eq. (7)

$$dx/d\xi = dx_e/d\xi + (1 - dx_e/d\xi) \cos kz. \qquad (8)$$

From Eqs. (1) and (5),

$$dx_e/d\xi = n(\xi)/n_u \qquad (9)$$

where

$$n_u = N k^2/P. \qquad (10)$$

We define the plasma frequency by $\omega_{p0}^2 = 4\pi e^2 n_u/m$. The distance the beam travels in one plasma period is $\lambda_{p0} = 2\pi v/\omega_{p0}$. Using Eqs. (4) and (10) we see that $\lambda_{p0} = 2\pi/k$ which is the same as λ, defined earlier.

Combining Eqs. (8) and (9),

$$dx/d\xi = n(\xi)/n_u + (1 - n(\xi)/n_u) \cos kz. \qquad (11)$$

Laminar motion ceases at the critical distance z_c where the left side vanishes:

$$\cos kz_c = \frac{-1}{n_u/n(\xi) - 1}. \qquad (12)$$

Laminarity Criterion: If $n(\xi) > n_u/2$ for all $\xi < h$, there is no solution; z_c does not exist, and the motion is laminar for all z in the cold beam limit.

If $n(\xi) \leq n_u/2$ over some range of ξ, then the part of the beam with the lowest density will cross trajectories first and define z_c. (This point of minimum n will be called ξ_c.) Beyond $z = z_c$, the linear equation (6) is invalid.

If z_c exists, then it always lies between $\lambda/4$ and $\lambda/2$.

Beam Density Time Dependence

Laminar motion implies $n(x,z)dx = n(\xi)d\xi$, so, using Eq. (11),

$$n(x,z) = \frac{n_u}{1 + (n_u/n(\xi) - 1)\cos kz} \qquad (13)$$

where the x dependence is found by simultaneous use of Eq. (7). Note that n(x) becomes uniform at $z = \lambda/4$ and then a density reversal occurs: particles originating in underdense regions find themselves in overdense regions and vice versa. If the laminarity criterion is violated, then $n \to \infty$ as $z \to z_c$ for particles originating at ξ_c. After z_c a shock-like phenomenon occurs which is illustrated in a later section.

If there are gaps in the density profile, then Eq. (11) needs some modification [5]. For such cases, $z_c = \lambda/4$.

For any cold-beam initial profile, continuous or not, matched or not, the density at $\lambda/4$ is uniform and equal to the density of a matched beam. This surprising and very important result comes from the linearity of Eq. (6) and is not quite true for round beams.

Rms Beam Size

Averages over density profiles are defined by

$$\langle g \rangle(z) = N^{-1} \int_0^\infty dx\, n(x,z)\, g(x). \qquad (14)$$

Changing the integration variable from x to the initial value ξ,

$$\langle g \rangle(z) = N^{-1} \int_0^\infty d\xi\, n(\xi)\, g(x(\xi,z)). \qquad (15)$$

For the mean-square beam width, we use the notation $X^2(z) = \langle x^2 \rangle$. Defining $C = \cos kz$ and using Eq. (7) we find

$$X^2(z) = \left[\frac{P}{\sqrt{3}\,k^2}(1-C) + X_0 C\right]^2 - U_{no}X_0\frac{P}{\sqrt{3}\,k^2}C(1-C). \qquad (16)$$

X_0 is the initial value of X and U_{no} is the initial value of the beam shape factor (which is zero for a uniform beam):

$$U_n(z) = 2 - 2\sqrt{3}\,W/PX \qquad (17a)$$

where

$$W(z) = P\langle x N_x \rangle / N \qquad (17b)$$

is the virial moment [3]. For discussion, see Ref. [5] which gives a table of U_n values; U_n is the normalized free self-field energy for a sheet beam.

Eq. (16) is greatly simplified for a matched beam.

Matching

In Eq. (16), whatever value of X_0 is chosen there will be fluctuations in X (unless the initial profile is uniform). But certain choices give a matched beam in the sense that the fluctuations are quite small. A particularly simple choice gives what we call $\lambda/4$ matching: we choose X_0, the value of X at $z = 0$, to be equal to the value given by Eq. (16) at $z = \lambda/4$:

$$X_0^2 = X^2(\lambda/4) = (P/k^2)^2/3 \qquad (18)$$

and Eq. (16) simplifies to

$$X^2(z) = X_0^2\left[1 - U_{no}\cos kz\,(1 - \cos kz)\right]. \qquad (19)$$

Eq. (18) gives the same matching as the equivalent beam approach [1,2,4]. Reference [5] also describes another type of matching which gives less than half the ripple.

Rms Emittance

We use Sacherer's definition of rms emittance [2]

$$\epsilon^2 = \langle x^2 \rangle \langle x'^2 \rangle - \langle x\,x' \rangle^2. \qquad (20)$$

We have already found $\langle x^2 \rangle$ [Eq. (16)]. The other moments may be found in the same way. When they are inserted in Eq. (20) many terms cancel, leading to a simple expression valid whether the beam is matched or not [5]. If we specify that the beam is $\lambda/4$ matched then we can write

$$\epsilon^2(z) = \frac{P}{\sqrt{3}}X_0^3\,U_{no}\left(1 - \frac{U_{no}}{4}\right)\sin^2 kz. \qquad (21)$$

This may be compared with the result from moments [5],

$$\frac{d}{dz}\epsilon^2 = -\frac{P}{\sqrt{3}}X^3(z)\frac{d}{dz}U_n. \qquad (22)$$

The factor $(1 - U_{no}/4)$ for typical initial beam profiles is usually within about 1% of unity. This factor arises from the small variations of X given by Eq. (19).

If the laminarity criterion is satisfied, then $\epsilon(z) \sim |\sin kz|$ indefinitely, as in Fig. 1a, where the initial profile is $n/n_u = 1.2 - 0.6\xi^2$ for $\xi \leq 1$, and 0 for $\xi > 1$.

There are two types of profiles which develop non-laminarity: (1) profiles with gaps and (2) continuous profiles. We discuss these cases in the next two sections.

Profiles with Gaps; Merging Beams

If there are gaps in the initial beam density profile, the emittance jumps to a substantial value at $z = \lambda/4$ and stays essentially constant thereafter. The physical basis for this phenomenon is discussed in Ref. [5].

Fig. 1b, obtained by numerical simulation [7], illustrates the effect. It shows ϵ vs. z/λ for 6 beams injected into one channel; the typical parameters are discussed in Ref. [5]. The emittance up to $z/\lambda = 1/4$ agrees with our next analytic result.

To analyze the emittance for a profile with gaps, we choose the simplest model: M segments each having the

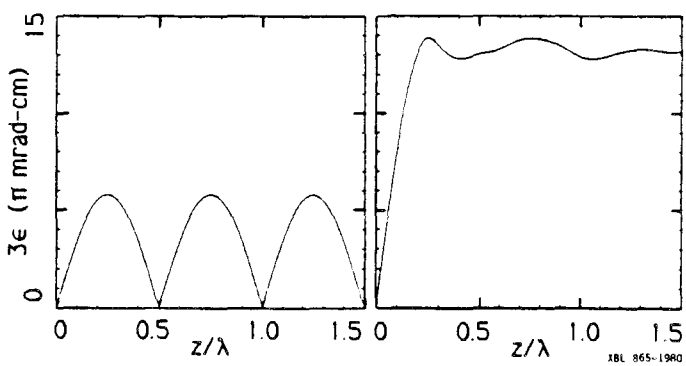

Fig. 1. Oscillatory and non-oscillatory emittances.
(a) Initial profile satisfies laminarity criterion.
(b) Merging beams with gaps in profile. See text.

same uniform density and the same width, and separated by distances equal to this width. For $\lambda/4$ matching we find [5]

$$\epsilon(z) = \frac{p^2}{3k^3}\,\frac{1}{M}\left[\frac{M^2-1}{4M^2-3}\right]^{1/2}\sin kz$$

for $z \lesssim \lambda/4$. The factor before sin kz equals 0.5 with correction < 1% for $M > 3$. In most practical cases, $\epsilon \sim 1/M$. Putting in numbers (see Ref. [5]), one finds that segmented beam emittances can jump to undesirably large values unless M, the number of beamlets, is large. This jump could occur in beam merging as proposed recently for some applications involving sheet beams or round beams. Our results indicate what could happen in either case: prompt, permanent and substantial emittance growth.

Continuous Profiles; Wave Breaking

In this section we discuss cases where $n(\xi)$ is non-vanishing out to the beam edge but $n(\xi) < n_u/2$ for some ξ; Eq. (12) gives the point $z = z_c$ where the trajectories will cross. As we have shown, the phase space dynamics of cold beams are easily and exactly described up to this point. Before z_c is reached, the distribution on the (x,x′) phase plane is a well-behaved curve with slope

$$\frac{dx'}{dx} = \frac{dx'/d\xi}{dx/d\xi} = \frac{-(1-n(\xi)/n_u)\,k\sin kz}{n(\xi)/n_u + (1-n(\xi)/n_u)\cos(kz)}. \quad (23)$$

Comparing with Eq. (12) shows that this slope is finite for $z < z_c$ so that $x'(x)$ is single valued. As $z \to z_c$ the curve steepens like the shape of a wave about to break. Although this occurs in phase space, not real space, the subsequent behavior is sometimes referred to as wave-breaking [6]. The effect in real space (for a cold beam) is that the charge density becomes singular as $z \to z_c$ [Eq. (13)]. After this singularity Eq. (6) must be replaced by (3).

Although our main purpose here is to present analytic results, we illustrate the effect with a typical numerical simulation [7]. The initial density profile was chosen to be $n/n_u = 1 - 0.7\cos(\pi\xi/h)$ for $\xi \lesssim h$, with $n = 0$ for $\xi > h$. Fig. 2 shows the steepening of dx′/dx and the wave-breaking in phase space. It also shows the corresponding density profiles which exhibit phenomena resembling shock fronts propagating from the singularity.

The rms emittance up to $z = z_c$ agrees with Eq. (21). Later its behavior is intermediate between Figs. 1a and 1b, showing damped oscillations. Very much later, the beam may reach equilibrium; equilibrium profiles are nearly uniform for space charge dominated beams. Ref. [5] shows that a uniform beam has minimum self-field energy for a given X. The final steady state for a matched beam would have about the same rms emittance as at the initial peak; this is shown at the end of the next section.

Thermal and Asymptotic Emittance

We can divide any mean-square emittance into a thermal part and a fluid-flow part [5]. We use the symbol $(\ldots)_{av}$ to denote a local average over velocities. For any value of x we define the fluid velocity $u(x,z) = (x')_{av}$ and the specific stress tensor $T(x,z) = ((x'-u)^2)_{av}$, which gives the temperature if the distribution is thermal. Then

$$\epsilon^2(z) = \langle x^2\rangle\langle T\rangle + \left[\langle x^2\rangle\langle u^2\rangle - \langle x\,u\rangle^2\right]. \quad (24)$$

For a cold beam during the period of laminar particle motion, given by Eq. (12), all the emittance is due to the flow term in brackets. But in general we have

$$\epsilon^2_{total} = \epsilon^2_{thermal} + \epsilon^2_{fluid}. \quad (24')$$

For warm beams we show in Ref. [5] that Eq. (21) still applies, at least up to $z = \lambda/4$, to the fluid part of the emittance if a slight correction is made to k. For matched beams (X nearly constant) the thermal term in Eq. (24′) is essentially constant; for our initial conditions $\epsilon_{therm}(z) = \epsilon_0$ and

$$\epsilon_{tot}(z) = \left[\epsilon_0^2 + \frac{p}{\sqrt{3}}X_0^3\,U_{no}\sin^2 k_1 z\right]^{1/2} \quad (25)$$

where k_1 is the slightly corrected wave number discussed in Ref. [5].

Eq. (25) resembles a sheet-beam version of an equation due to Struckmeier, Klabunde and Reiser -- see Eq. (15) in Ref. [4]. What is new in Eq. (25) is that it shows that the upper limit mentioned in [4] is actually reached and shows that it is reached at $z \approx \lambda_0/4$.

If wave-breaking occurs, then energy is transferred from the fluid term to the $\langle T\rangle$ term, in a non-thermal way at first. Asymptotically, complete thermalization could occur. For any time scale, we can use the invariant (twice the total energy) [8]:

$$\langle T\rangle + \langle u^2\rangle + k^2\langle x^2\rangle - 2W(z) = \text{Const} \quad (26)$$

where W(z), the virial moment, is related to $U_n(z)$; see Eq. (17). If the beam becomes more uniform, W increases and

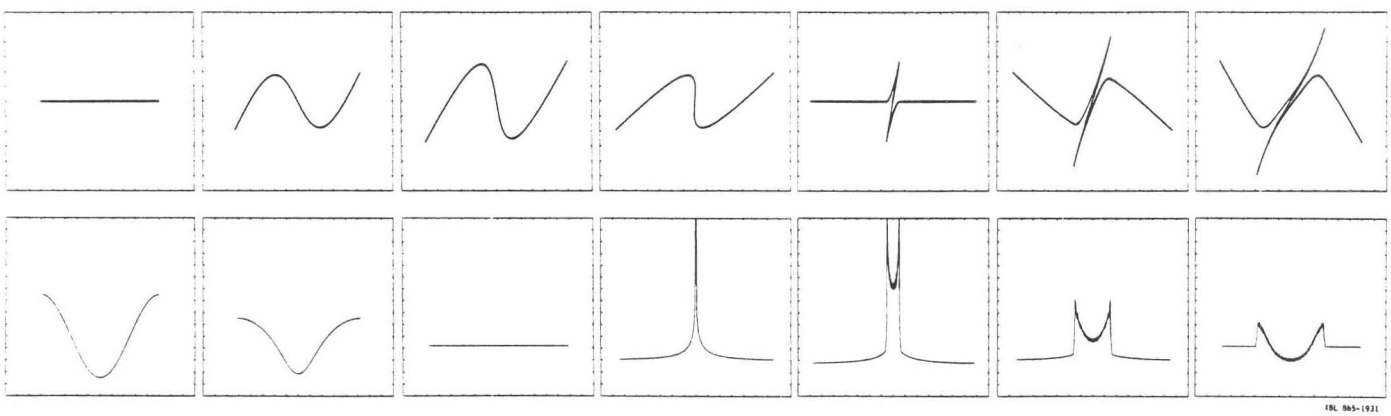

Fig. 2. Example of wave breaking in phase space and shock formation in configuration space; $z/\lambda = 0.0$, 0.125, 0.25, 0.375, 0.5, 0.625, and 0.75. Upper row shows phase plots; lower row shows corresponding charge densities. These results during the laminar regime agree with Eqs. (23) and (13). According to Eq. (12) wave-breaking starts at $z_c = 0.32\lambda$. This figure illustrates cold beam behavior. Space-charge dominated warm beams show similar patterns in the phase plane; their density profiles for $z \gtrsim z_c$ show similar shock-like structures but are smoother.

therefore so does $\langle u^2 \rangle$ or $\langle T \rangle$. Asymptotically, $u_\infty = 0$, and also $U_{n\infty} \approx 0$ to high accuracy for a space-charge dominated beam. Eqs. (24) and (26) yield

$$\epsilon_\infty = \frac{X_\infty}{X_0}\left[\epsilon_0^2 + \frac{P}{\sqrt{3}}X_0^3 U_{n0} + k^2 X_0^2(X_0^2 - X_\infty^2) + \frac{2P}{\sqrt{3}}X_0^2(X_\infty - X_0)\right]^{1/2}$$

and $\epsilon(\infty) \approx \epsilon(\lambda_1/4)$ if $X_\infty = X_0$. But see Ref. [8] if $X_\infty \neq X_0$.

II. ROUND BEAMS

Exact results are not obtainable for round beams, but perturbation analysis gives accurate results which are similar to those for sheet beams. We find:

(a) The critical density for laminar particle motion is again half the equivalent uniform density but with a first order correction, typically around 10%.

(b) Different parts of a non-uniform round beam oscillate at slightly different frequencies. The correction is of second order (usually less than one percent), with negligible effect except perhaps for long time scales. The frequency for a cold beam is essentially $2k^2$.

(c) The particle excursions are nonlinear, so the beam density is not precisely uniform at $z = \lambda_0/4$, where $\lambda_0 = 2\pi/\omega_0$. However, the nonuniformity is so small that essentially all the free self-field energy is converted into kinetic energy and emittance growth.

Again, we start with cold beams and discuss thermal effects later.

Particle Motion

If the beam density is $n(r,z)$, the number of particles per cm of length within radius r is

$$N_r(r,z) = \int_0^r 2\pi r\, n(r_1,z)\, dr_1 . \qquad (27)$$

The self field is $E_s = 2eN_r/r$ and the total perveance is

$$K = 2Ne^2/mv^2 \qquad (28)$$

where N is the total number per cm. The external focusing force is assumed to be linear:

$$r'' = -k^2 r + K N_r(r,z)/(N r) \qquad (29)$$

and for a cold beam the particle motion is laminar for z less than a critical distance z_c. We write ρ for the initial position of the particle that is currently at $r(z)$; thus $N_r(r,z) = N_r(\rho,0)$. Using the abbreviation $N_r(\rho,0) = N_r(\rho)$, we define the equilibrium position

$$r_e(\rho) = \left[\frac{K}{k^2}\frac{N_r(\rho)}{N}\right]^{1/2} \qquad (30)$$

so that

$$r'' + k^2(r - r_e^2/r) = 0 \qquad (31)$$

in the laminar range. This equation can be solved by the Lindstedt-Poincaré method discussed in [9]. The solution, for the initial condition $r'(\rho) = 0$, is

$$r(\rho,z) = r_e\left[1 + \delta\cos\omega z + \frac{\delta^2}{4}(1 - \frac{1}{3}\cos 2\omega z) + \cdots\right] \qquad (32)$$

where

$$\delta(\rho) = \eta - \eta^2/6 \qquad (33)$$

$$\eta(\rho) = \rho/r_e(\rho) - 1 \qquad (34)$$

$$\omega(\rho)/\omega_0 = 1 + \delta^2/12 \qquad (35)$$

$$\omega_0^2 = 2k^2. \qquad (36)$$

We can show that η vanishes for all ρ if the beam is matched and uniform; therefore η is a uniformity parameter. We only need it to first order in the following results, but second order terms must be kept in Eqs. (32) and (33) in order to derive those results [5].

Trajectory Crossing for Continuous Profile

As in the case of sheet beams, laminar particle motion ceases at the critical distance z_c where the derivative $dr(\rho,z_c)/d\rho$ vanishes. From Eqs. (27) and (30),

$$(r_e\, dr_e)/(\rho\, d\rho) = n(\rho)/n_u ; \qquad (37)$$

for round beams

$$n_u = N k^2/\pi K . \qquad (38)$$

Using Eq. (32), we find to first order in η

$$\frac{r\, dr}{\rho\, d\rho} = \frac{n(\rho)}{n_u} + \left[1 - \frac{n(\rho)}{n_u}\right]\left[C + \frac{2}{3}\eta(1 - C)^2\right] \qquad (39)$$

where $C = \cos\omega_0 z$. The condition for trajectory crossing is found by setting the left side equal to zero and solving for $\cos\omega_0 z_c$. Defining a as the initial beam edge (where the density falls to zero) we get the following:

Laminarity Criterion (to first order in η):

$$\text{If} \quad n(\rho) > \frac{n_u}{2}\left(1 - \frac{4}{3}\eta\right) \quad \text{for all } \rho < a,$$

then the motion is laminar for all z. The criterion is the same as for sheet beams except for the correction factor.

Beam Density Time Dependence

In analogy with sheet beams, laminarity can be expressed as

$$2\pi r n(r,z)dr = 2\pi\rho n(\rho)d\rho . \qquad (40)$$

Eq. (39) gives

$$n(r,z) = \frac{n(\rho)}{\frac{n(\rho)}{n_u} + \left[1 - \frac{n(\rho)}{n_u}\right]\left[C + \frac{2}{3}\eta(1 - C)^2\right]} \qquad (41)$$

where the r dependence is obtained by simultaneous use of Eq. (32). If the laminarity criterion is violated, shock-like behavior (similar to that in Fig. 2) will begin at $z = z_c$ if the initial profile is continuous.

Rms Beam Size and Matching

Equation (32) shows a complicated time behavior. We will not consider the exact time dependence of $R^2 = \langle r^2 \rangle$ but will only calculate it at $z = \lambda_0/4$, where

$$\lambda_0 = 2\pi/\omega_0 .$$

At this point the density profile is nearly uniform so that essentially all of the free self-field energy is converted into fluid energy.

Averages over density profiles are given by

$$\langle g \rangle(z) = N^{-1}\int_0^a d\rho\, 2\pi\rho\, n(\rho)\, g(r(\rho,z)) \qquad (42)$$

where we used Eq. (40) to change the integration variable from the current position r to the initial value ρ. The initial mean-square radius at $z = 0$ is

$$R_0^2 = \langle \rho^2 \rangle = N^{-1}\int_0^a d\rho\, 2\pi\rho^3\, n(\rho). \qquad (43)$$

At $z = \lambda_0/4$, Eq. (32) gives, to first order in η,

$$\langle r^2 \rangle(\lambda_0/4) = \langle r_e^2 \rangle . \quad (44)$$

From Eqs. (37) and (42), $\langle r_e^2 \rangle = K/2k^2$. It follows that the condition for $\lambda_0/4$ matching is

$$R_0^2 = K / 2k^2. \quad (45)$$

Peak Rms Emittance

In terms of the radius, Sacherer's x emittance, Eq. (20), is

$$\epsilon = \frac{1}{2}\left[\langle r^2 \rangle \langle r'^2 \rangle - \langle r r' \rangle^2\right]^{1/2} . \quad (46)$$

The above moments at $z = \lambda_0/4$ are readily evaluated from Eq. (32) to first order in η. But it is easier to calculate the peak emittance from the free self-field energy; Ref. [5] shows that the two methods give nearly identical results.

Our exact solution for sheet beams, Eq. (21), turned out to be closely related to a differential equation for emittance vs. free energy, Eq. (22). The analogous differential equation for round beams was given in Refs. [1], [3], and [4]. In Ref. [4], it was integrated by treating R as constant. This yielded a maximum emittance growth

$$\Delta\epsilon^2(\max) = K R_0^2 U_{n0} / 16 \quad (47)$$

where U_{n0} is the initial value of the normalized free self-field energy, given by

$$U_n(z) = 4\int_0^b dr\, N_r^2(z)/ N^2 r - (1 + 4 \ln b/R\sqrt{2}). \quad (48)$$

(One chooses b to include all the beam.) The analysis used in [1,3,4] did not show how rapidly the maximum emittance would be reached. But if, as in Part I, the density profile at $z = \lambda_0/4$ is essentially uniform, then we find

$$\epsilon^2(\lambda_0/4) = K R_0^2 U_{n0} / 16. \quad (49)$$

We have confirmed such uniformity for typical profiles. An example is the parabolic profile:

$$n(\rho) = \frac{2N}{\pi a^2}\left[1 - \frac{\rho^2}{a^2}\right]. \quad (50)$$

In Ref. [5] we found analytically the density profile at $z = \lambda_0/4$ as an explicit function of r. The result is plotted in Fig. 3 where it is compared with the initial profile. The density is clearly flat enough at $z = \lambda_0/4$ to make $U_n(z)$ negligible. Thus, Eq. (49) gives an accurate result.

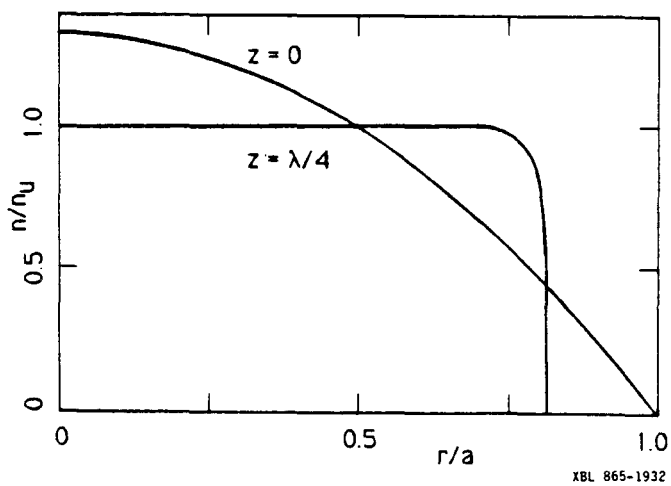

Fig. 3. Analytic density profiles at $z = 0$ and $z = \lambda_0/4$.

To confirm this point, we calculated the emittance at $z = \lambda_0/4$ using the free energy U_{n0}, Eq. (48), and compared it with the result obtained from the dynamics using Eqs. (32) and (46). We found $\epsilon(\lambda_0/4) = 0.0374\, R_0\sqrt{K}$ using the first method, and $0.0375\, R_0\sqrt{K}$ using the second. The uniformity at $\lambda_0/4$ (Fig. 3) is responsible for the high accuracy of the free energy calculation.

Thermal and Asymptotic Emittance

For matched, strongly space-charge dominated beams the total emittance at $z \approx \lambda_0/4$ is

$$\epsilon_{peak} = \left[\epsilon_0^2 + \frac{K}{16} R_0^2 U_{n0}\right]^{1/2} . \quad (51)$$

See the discussion in the last section of Part I. Simulation studies by C.M. Celata [10] have confirmed that Eq. (51) gives accurate results for a space-charge dominated beam. Our prediction that the emittance peaks at $z \approx \lambda_0/4$ agrees with the simulations reported by Wangler et al. [4]; in fact, the present study was inspired by a desire to understand the physics behind those surprising results.

The invariant corresponding to Eq. (26) is [8]

$$\langle T_r \rangle + \langle u_r^2 \rangle + k^2 \langle r^2 \rangle + K U_n(z)/4 - K \ln R = \text{Const.}$$

where u_r and T_r are radial versions of the quantities in Eq. (24), and $U_n(z)$ is defined by Eq. (48). For the asymptotic case discussed under Eq. (26) we have $u_r = 0$, $T_r \approx 0$, and

$$\epsilon_\infty = \frac{R_\infty}{R_0}\left[\epsilon^2_{peak} + \frac{k^2}{4} R_0^2 (R_0^2 - R_\infty^2) + \frac{K}{4} R_0^2 \ln \frac{R_\infty}{R_0}\right]^{1/2}$$

which agrees with Ref. [4] if $R_\infty = R_0$. We can eliminate R_∞ for cases where the beam size is mismatched [8]. The result is the same as in [4] but with additional terms.

Acknowledgments

I wish to thank Chris Celata, Ed Lee, and Denis Keefe for their valuable advice and encouragement. And although the present paper concentrates on analytic results, numerical simulations were a valuable adjunct and I am grateful for the enthusiastic collaboration of Ludmilla Soroka. This work was supported by US DOE Contract DE-AC03-76SF00098.

References

[1] P.M. Lapostolle, CERN-ISR-DI/71-6 (1971).
P.M. Lapostolle, IEEE Trans. Nucl. Sci., 18, 1101 (1971).
[2] F.J. Sacherer, IEEE Trans. Nucl. Sci., 18, 1055 (1971).
[3] E.P. Lee, S.S. Yu, and W.A. Barletta, Nuclear Fusion, 21, 961 (1981).
[4] T.P. Wangler, K.R. Crandall, R.S. Mills, and M. Reiser, IEEE Trans. Nucl. Sci., 32, 2196 (1985). This paper lists many other important references. It is partly based on: J. Struckmeier, J. Klabunde, and M. Reiser, Particle Accel., 15, 47 (1984).
[5] O.A. Anderson, "Internal Dynamics and Emittance Growth in Space-Charge Dominated Beams," Particle Accel., to be published.
[6] I.B. Bernstein and S.K. Trehan, Nuclear Fusion, 1, 3 (1960). The section on non-linear oscillations is based on the work of John Dawson. See references.
[7] O.A. Anderson, D.G. Kane, and L. Soroka, Bull. Am. Phys. Soc., 30, 1595 (1985).
[8] O.A. Anderson, International Symposium on Heavy Ion Fusion, Washington, D.C., May 27-29, 1986. Proceedings to be published by AIP.
[9] A.H. Nayfeh and D.T. Mook, Nonlinear Oscillations, John Wiley and Sons, New York, 1979.
[10] C.M. Celata, personal communication, Lawrence Berkeley Laboratory, December 1985.